Inorganic Chemistry

Article

pubs.acs.org/IC

Two Homologous Intermetallic Phases in the Na–Au–Zn System with Sodium Bound in Unusual Paired Sites within 1D Tunnels

Saroj L. Samal, Qisheng Lin, and John D. Corbett*

Ames Laboratory-DOE and Department of Chemistry, Iowa State University, Ames, Iowa 50010, United States

Supporting Information

ABSTRACT: The Na–Au–Zn system contains the two intermetallic phases $Na_{0.97(4)}Au_2Zn_4$ (**I**) and $Na_{0.72(4)}Au_2Zn_2$ (**II**) that are commensurately and incommensurately modulated derivatives of $K_{0.37}Cd_2$, respectively. Compound **I** crystallizes in tetragonal space group *P*4/*mbm* (No. 127), a = 7.986(1) Å, c = 7.971(1) Å, Z = 4, as a 1 × 1 × 3 superstructure derivative of $K_{0.37}Cd_2$ (*I*4/*mcm*). Compound **II** is a weakly incommensurate derivative of $K_{0.37}Cd_2$ with a modulation vector q = 0.189(1) along c. Its structure was solved in superspace group *P*4/*mbm*(00*g*)00ss, a = 7.8799(6) Å, c = 2.7326(4) Å, Z = 2, as well as its average structure in *P*4/*mbm* with the same lattice parameters.. The Au–Zn networks in both consist of layers of gold or zinc squares that are condensed antiprismatically along c ($[Au_{4/2}Zn_4Zn_4Au_{4/2}]$ for **I** and $[Au_{4/2}Zn_4Au_{4/2}]$ for **II**) to define fairly uniform tunnels. The long-range cation dispositions in the tunnels are all clearly and rationally defined by electron density (Fourier) mapping. These show only close, somewhat diffuse, pairs of opposed, ≤50% occupied Na sites that are centered on (**I**) (shown) or between (**II**) the gold squares. Tight-binding electronic structure calculations via linear muffin-tin-orbital (LMTO) methods, assuming random occupancy of ≤ ∼100% of nonpaired Na sites, again show that the major Hamilton bonding populations in both compounds arise from the polar heteroatomic Au–Zn interactions. Clear Na–Au (and lesser Na–Zn) bonding is also evident in the COHP functions. These two compounds are the only stable ternary phases in the (Cs,Rb,K,Na)–Au–Zn systems, emphasizing the special bonding and packing requirements in these sodium structures.

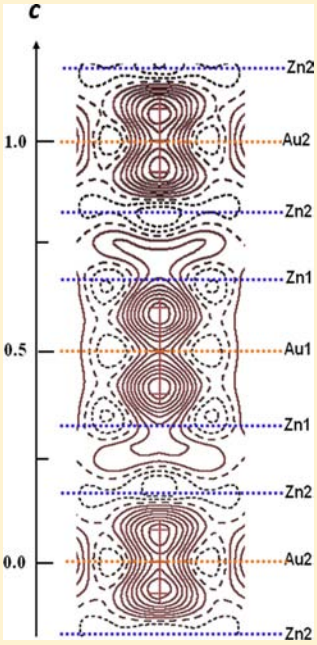

INTRODUCTION

A rich variety of fascinating structures with diverse clusters and networks and novel bonding features are observed among polar intermetallic compounds. The ternary examples often contain an electropositive alkali (A) or alkaline-earth (Ae) metal, a relatively electronegative late transition metal, gold in particular, and a main group metal or metalloid. Such compounds are electronically situated between Zintl and Hume–Rothery phases, and those closer to the former often exhibit high coordination number environments for the network atoms and more delocalized bonding than in the more classical Zintl phases.[1−3] Gold affords a particularly large and diverse variety of novel examples in A/Ae–Au–Tr systems (Tr = triel = Ga, In, Tl).[4−13] Furthermore, early investigations indicated that phase diversities and atom coordination numbers generally increase when the post-transition components are replaced by late transition metals such as Cd, Zn, Cu, etc. in place of Tr.[14,15] Thus, the Na–Au–Cd system yielded a novel condensed cluster network $Na_6Cd_{16}Au_7$, (isotypic with $Mg_6Cu_{16}Si_7$, despite the chemical contrasts) that contain segregated tetrahedral stars of Cd networked with individual Au atoms.[14] Switches of the alkali-metal components to the alkaline-earth (or to rare-earth) metals with the higher field ions always produce substantial differences, particularly better ordered and more regular structures.[15−18] Certain less tightly bound alkali-metal systems also allow the formation of what may be described as zeolitic phases, or at least tunnel structures that resemble these, even though the characteristic ion exchange properties have not yet been established. Relative cation and network sizes and proportions appear critical for zeolitic structure formation. Only a few intermetallic phases with open tunnel structures are known to date,[6,19−22] and most of these bind more or less disordered cations with fractional occupancies. Among A–Au–In systems (A = Na, K, Rb), the gold-rich KAu_4In_2 contains mixed Au, In tunnels centered by K, with no evident cation disorder or vacancies.[6] In contrast, sodium-richer compounds in the Na–Au–In systems exhibit quite different anionic frameworks.[9−11,23,24] In Na_3AuIn_2,[11] Au–In tetrahedral star (TS) $[In_4Au_{4/2}]$ units are connected into a three-dimensional (3D) frameworks via shared TS vertexes, whereas in $Na_2Au_6In_5$,[10] the Au and In atoms define condensed, indium-centered Au_{12} icosahedra and empty Au_6 octahedra in a CsCl-like arrangement.

Received: June 5, 2012
Published: August 20, 2012

   dx.doi.org/10.1021/ic301196z | *Inorg. Chem.* 2012, 51, 9395–9402

Table 1. Selected Crystal Data and Structure Refinement Parameters for $Na_{0.97}Au_2Zn_4$ and $Na_{0.72}Au_2Zn_2$

		$Na_{0.72(4)}Au_2Zn_2$ (II)	
compound	$Na_{0.97(4)}Au_2Zn_4$ (I)	average	incommensurate
formula weight	678.56	543.14	543.14
space group, Z	$P4/mbm$ (No. 127), 4	$P4/mbm$ (No. 127), 2	$P4/mbm(0\,0\,g)00ss$ $q = (0\,0\,0.189)$
unit-cell parameter	a = 7.9859(4) Å, c = 7.9709(8) Å	a = 7.8799(6) Å, c = 2.7326(4) Å	a = 7.8799(6) Å, c = 2.7326(4) Å
V	508.35(6) Å^3	169.67(3) Å^3	169.67(3) Å^3
d_{calcd}	8.86 g/cm^3	10.72 g cm^{-3}	10.72 g cm^{-3}
Refl. coll./R_{int}	4118/0.0547	1366/0.0496	1386/0.1915
μ	75.97 mm^{-1} (Mo Kα)	99.99 mm^{-1} (Mo Kα)	99.99 mm^{-1} (Mo Kα)
data/parameters	370/25	143/11	181/27
GOF on F^2	0.877	1.115	1.04
R_{all} (R/R_w)[a] ($I > 2\sigma$)	0.0261/0.0768	0.0207/0.0496	0.0643/0.0871
(all data)	0.0297/0.0799	0.0233/0.0506	0.1322/0.1125
R_{main} (R,R_w) ($I > 2\sigma$)			0.0386/0.0598
(all data)			0.0553/0.067
$R_{satellite}$ (R,R_w) ($I > 2\sigma$)			0.1694/0.3007
(all data)			0.3246/0.4013
diff. peak, hole	1.64 e Å^{-3}/−1.66 e Å^{-3}	1.91 e Å^{-3}/−1.60 e Å^{-3}	3.00 e Å^{-3}/−2.78 e Å^{-3}

[a] $R = \sum||F_0| - |F_c||/\sum|F_0|$; $R_w = [\sum w(|F_0| - |F_c|)^2/\sum w(F_0)^2]^{1/2}$; $w = 1/\sigma_F^2$.

The novel tunnel structures in K/Rb−Au−In systems,[6,22] in great contrast with the rigid $Na_6Cd_{16}Au_7$ above, motivated us to extend our explorations to the A−Au−Zn systems, for which there are no reports of such ternary phases. Here, we describe two new compounds with linear tunnels that are populated by new varieties of somewhat diffuse but locally ordered Na cation distributions. This study has also taken place more or less in parallel with investigations of a range of the neighboring A−Au−Ga systems (A = Na−Cs), in which more-extended versions of similar cation−tunnel problems have been encountered and clarified.[12,13] The requisite narrow tolerances on atom sizes and stoichiometries are important in all of these.

EXPERIMENTAL SECTION

Syntheses. All reactants and products were handled in a glovebox filled with dry N_2 (≤0.1 ppm H_2O per volume). The compounds were synthesized via high-temperature reactions of the elemental gold (99.995%, Ames Lab), zinc (99.99%), and sodium (99.9%), the last two from Alfa Aesar. The weighed reactants were weld-sealed into tantalum containers that were subsequently enclosed in evacuated silica jackets to protect the Ta from heated air. The elements were allowed to react at 650 °C for 12 h, quenched, equilibrated at 450 °C for 4 days, and then cooled to room temperature. (Longer equilibrations gave the same results.) Single crystals of **I** and **II** were first obtained from reactions loaded as $NaAuZn_2$ and $NaAu_2Zn_2$, respectively. Then, single-phase (X-ray pure) samples of each were obtained from syntheses according to the stoichiometries determined from single-crystal refinements, as verified by the very close agreement between the observed powder X-ray diffraction (XRD) patterns and those calculated from the refined structural data for each (see Figure S1 in the Supporting Information). These correspondences between powder patterns, and between compositions loaded and structural compositions refined, afford powerful evidence for the stoichiometries of the products, far better than can usually be achieved instrumentally by a microprobe EDS analysis, etc.

In order to check for homogeneity regions for both phases, several compositions were reacted under the same conditions, keeping the anion proportions fixed and varying the cation contents; however, only shifts in unit-cell parameters within acceptable 3σ limits were observed for both. The compounds have metallic lusters and turn black within ∼15 min in moist air at room temperature. Stable ternary Na−Au−Zn products are limited to the two reported here. Furthermore, attempts to find new compounds in the neighboring (K,Rb,Cs)−Au−Zn systems under similar reaction conditions always ended up with significant phase segregation into stable binaries of Au and Zn plus unreacted alkali metals.

X-ray Diffraction Studies. Powder diffraction data were collected at room temperature with the aid of a Huber 670 Guinier powder camera equipped with an area detector and Cu Kα radiation (λ = 1.54059 Å). The samples were dispersed between two Mylar sheets with the aid of a small amount of vacuum grease. These were, in turn, held between split Al rings that provided airtight seals. The lattice parameters were refined with the aid of the WinXPow program.[25]

Crystals of **I** ($Na_{0.97(4)}Au_2Zn_4$) and **II** ($Na_{0.72(4)}Au_2Zn_2$) were sealed in capillaries in a N_2-filled glovebox and then mounted on a Bruker SMART CCD diffractometer equipped as a Mo Kα radiation source (λ = 0.71073 Å). Single-crystal diffraction data sets were collected at room temperature as three sets of 606 frames with 0.3° scans in ω and exposure times of 10 s per frame over the 2θ range from ∼3° to ∼57°. The reflection intensities were integrated with the SAINT program in the SMART software package.[26] Empirical absorption corrections were made with the aid of the SADABS program.[27] The space group determinations were done with the aid of XPREP and SHELXTL 6.1.[28] Systematic absences suggested tetragonal space group $P4/mbm$ (No. 128) for both compounds. The structures were solved by direct methods and subsequently refined on $|F^2|$ with a combination of least-squares refinement and difference Fourier maps.

Conventional direct methods first yielded four independent atomic positions for **I** with suitable separations for Au/Zn−Au/Zn pairs, so they were initially assigned to Au1−Au4, respectively. The large isotropic displacement parameters obtained for the last two positions suggested lighter atoms, and these were hence assigned as Zn1 and Zn2 and suitably refined. After several cycles of refinement, two more less-populated sites with reasonable Na−Au/Zn distances were gained with the aid of difference Fourier maps and were so assigned to Na1 (2a) and Na2 (2b) and refined. Ultimately, four independent Na sites were located from electron density (e.d.) maps and peak-picking routines, all along 0 0 z in the center of the tunnels defined by Au and Zn atoms. All Na had enlarged isotropic parameters, and Na3 and Na4 (4e) were slightly displaced from observed electron density centers (see discussion below). These problems are quite similar to those recently encountered with related tunnel structures in the $A_{\sim 0.5}Au_2Ga_2$ systems,[12,13] namely, that anisotropic displacement parameters refined for such problematic cations were all markedly elongated along c (the tunnel direction), overlapping those centered on other cations. More plausible isotropically refined parameters were still large and the 4e cation sites were not always at the centers of the respective electron

dx.doi.org/10.1021/ic301196z | Inorg. Chem. 2012, 51, 9395−9402

Table 2. Atomic Coordinates and Isotropic Equivalent Displacement Parameters for $Na_{0.97(4)}Au_2Zn_4$ (I)

atom	Wyckoff	x	y	z	U_{eq} [Å^2]	Occ ≠1
Au1	4h (*m*.2*m*)	0.6664(1)	0.1664(1)	0.50000	0.0182(4)	
Au2	4g (*m*.2*m*)	0.3658(1)	0.1342(1)	0.00000	0.0167(4)	
Zn1	8k (*m*)	0.3691(2)	0.1308(2)	0.3331(2)	0.0185(6)	
Zn2	8k (*m*)	0.6659(2)	0.1659(2)	0.1665(3)	0.0197(6)	
Na1	2a (4/*m*)	0.0000	0.0000	0.0000	0.04[a]	0.51(4)
Na2	2b (4/*m*)	0.0000	0.0000	0.5000	0.04[a]	0.48(4)
Na3	4e (4/*m*)	0.0000	0.0000	0.111(1)	0.04[a]	0.21(2)
Na4	4e (4/*m*)	0.0000	0.0000	0.329(1)	0.04[a]	0.27(3)

[a]Fixed parameters.

Table 3. Atomic Coordinates and Isotropic Equivalent Displacement Parameters Refined for $Na_{0.72(4)}Au_2Zn_2$ (II) in the Average Structure *P4/mbm* and for $Na_{0.93(10)}Au_2Zn_2$ in Super-space Group *P4/mbm*(00*g*)00*ss*, *q* = 0.189

atom	Wyckoff	x	y	z	U_{eq} [Å^2]	Occ ≠ 1[a]
Commensurate						
Au	4g	0.17436(4)	$-x$ + 1/2	0	0.0138(2)	
Zn	4h	0.1235(1)	x + 1/2	1/2	0.0136(4)	
Na	4e	1/2	1/2	0.346(1)	0.04[a]	0.36(4)
Incommensurate						
Au	4g	0.1735(3)	$-x$ + 1/2	0	0.0073(3)	
Zn	4h	0.1219(10)	x + 1/2	1/2	0.0093(7)	
Na	2b	1/2	1/2	1/2	0.06(2)	0.93 (10)

[a]Fixed value.

densities in the Fourier map. These are clear indications of the coexistence of both occupancy and configurational disorder. Ultimately, the structure was provisionally refined conventionally for the heavy atoms plus the four Na atoms with fixed U_{iso} = 0.04 Å^2 in two 4*e*, 2*a*, and 2*b* sites, two *z* parameters for the first pair, and four occupancy variables of ∼0.25 or ∼0.5, depending on the site, with standard deviations for the last of ∼10%). This approach appears to give the most meaningful evaluation of the composition, but the 2 + 2 sets of Na positions did not describe a reasonable atom disposition. (These sites in **I** are also shown superimposed on the later Fourier mapping results in Figure S2 in the Supporting Information.)

The final refinements of **I** yielded (R = 0.0297, wR = 0.0789, goodness of fit (GOF) = 0.877; 25 parameters, 370 independent observed reflections (see Tables 1 and 2). The refined composition $Na_{0.97(4)}Au_2Zn_4$ was suitably close to the loaded (1.015:2:4) proportions. Because the evident cation disorder problems are similar to those in the known incommensurate structure of $Sc_4Mg_xCu_{15-x}Ga_{7.5}$,[21] we also checked as to whether **I** also exhibited evidence for incommensurate modulation. However, no clue for such a possibility was observed after data collection on a STOE IPDS II diffractometer with exposures of 7 min per frame. The much better description of the sodium distributions via e.d. mapping will be presented later in the Results and Discussion section after the basic structure has been described.

Compound **II** was initially solved in the same *P4/mbm* group, Z = 2, with a = 7.8799(6) Å, c = 2.7326(4) Å as a structure with three independent atom positions. However, similar to the behavior of **I**, both the refined anisotropic displacement ellipsoids and the distances between the evidently fractional Na atoms were arguable, i.e., U_{33} = 0.71(5) versus U_{11} = U_{22} = 0.014(3) and 2.78 Å separations. For comparison, a more conventional refinement, isotropic for Na with U_{iso} again fixed at 0.04, converged at a composition of $Na_{0.72(4)}Au_2Zn_2$ with R = 0.0207, R_w = 0.0496, GOF = 1.115 for 11 parameters and 143 independent observed reflections, similar to the results obtained for **I** (see Table 3).

The same crystal of **II** was also checked with the aid of a Stoe IPDS-II diffractometer with exposures of 8 min per frame to determine whether an incommensurate structure was present. A reciprocal space view of the [*h* 5 *l*] zone (Results section, Figure 1) contained weak but clear reflections above and below the main reflections that could be

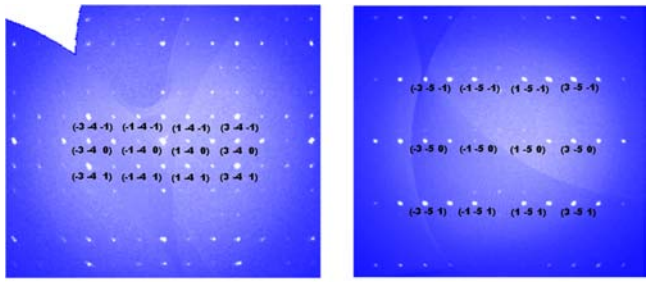

Figure 1. Reflections in reciprocal space for (a) $Na_{0.97(4)}Au_2Zn_4$ (**I**); (b) weak reflections above and below main reflection in $Na_{0.72(4)}Au_2Zn_2$ (**II**).

indexed with a modulation vector q = 0.189(1) along *c*. Therefore, the intensity data were indexed with (3 + 1) parameters with the aid of X-RED program, and then imported into program JANA2006.[29] Numerical absorption corrections were made with the help of X-Shape.[29] The superspace group *P4/mbm*(00*g*)00*ss* was suggested by Superflip,[30] which also yielded the incommensurate structural model (with a consideration of twin components). Least-square refinements were carried out with the help of the same program. Table S1 in the Supporting Information lists detailed information about data collection and structural refinements. Both Au and Zn atoms exhibit strong positional displacements in the *x*- and *y*-directions that could be modeled by harmonic functions. In contrast, Na atoms in the superspace group remain linearly positioned in tunnels with position modulations in *z*, and they exhibited occupancy modulations that could be described with crenel functions. The sine and cosine parameters in all three directions used for description of the incommensurate modulations of these three atoms are given in Table S2 in the Supporting Information. It should be noted that the R factors for satellite reflections alone are appreciable (R_{obs} ≈ 16.9%), because of the weak modulation—only 80 out of 180 satellite reflections were classified as observed. Nevertheless, the incommensurate structural model is reasonable, as supported by the good agreement between F_0 and F_c (see Figure S3 in the Supporting Information). The refined composition is $Na_{0.93(10)}Au_2Zn_2$, in which

dx.doi.org/10.1021/ic301196z | Inorg. Chem. 2012, 51, 9395−9402

the Na proportion is ~2σ from that refined in average structure, 0.72(4); the large standard deviation for the Na occupancy is due to the fact that it has large correlations with U_{11} and with the z-sine modulation. Therefore, in the following, $Na_{0.72(4)}Au_2Zn_2$ is referred to as phase **II**. The results for and further analyses of the model for the average structure of **II** in tetragonal *P4/mbm* are reported and discussed in the Results section for comparisons with compound **I** and related structures.

Data for the foregoing appear in Tables 1−3, and important bond distances in both phases are given in Tables S5 and S6 in the Supporting Information. The anisotropic displacement parameters for all independent heavy atoms are listed in Tables S3 and S4 in the Supporting Information. The cif outputs also appear therein.

Electronic Structure Calculations. In order to better understand the bonding characteristics and the relativistic effects on Au bonding, tight binding calculations were performed for both phases, according to the linear-muffin-tin-orbital (LMTO) method in the atomic sphere approximation (ASA).[31] The radii of the Wigner−Seitz spheres were assigned automatically such that the overlapping potentials would be the best possible approximations to the full potential.[32] One additional empty sphere per unit cell was needed for both **I** and **II** subject to an 18% overlap restriction with atom-centered spheres. Calculations for $NaAu_2Zn_4$ and the idealized $Na_{0.5}Au_2Zn_2$ were performed with nonadjacent halves of the split cation sites fully occupied (below); different choices among these did not matter. Basis sets of Na 3s,3p, (3d), Au 6s,6p,5d,(5f), Zn 4s,4p (downfolded orbitals in parentheses) were employed, and the reciprocal space integrations were performed on grids of 1728 irreducible k-points. Scalar relativistic corrections were included. For bonding analysis, the energy contributions of all filled electronic states for neighboring atom pairs were calculated by the crystal orbital Hamilton population (COHP) method.[33] The calculations avoided the problematic occurrence of close pairs of 50% Na atoms by removing the mirror planes normal to c through use of space group *P4bm*, inputting either *cis* or *trans* pairs of 100% Na on adjacent dimer sites. Both gave essentially the same answer (see the Results section). The COHP data for each atom pair (which are negative for bonding interactions) were given weighted integrations up to E_F to provide ICOHP values and Hamilton overlap populations, which are approximations of relative bond populations (see Tables 4 and 5).

Table 4. Bond Length Ranges and Average and Combined Molar ICOHP Data for $Na_{0.97(4)}Au_2Zn_4$ (I) (Z = 4)

bond	length (Å)	−ICOHP (avg.) (eV/per bond)	n/cell	−ICOHP (eV/cell)	contribution (%)
Au−Zn	2.619−2.753	1.30	64	83.2	62.6
Zn−Zn	2.651−2.957	1.16	36	41.76	31.4
Au−Au	3.032	0.68	2	1.36	1.0
Na−Au	3.011−3.145	0.18	16	2.88	2.2
Na−Zn	3.104−3.601	0.11	32	3.56	2.8

RESULTS AND DISCUSSION

Crystal Structures. Judging from lattice parameters, space groups, and structural features, both $Na_{0.97(4)}Au_2Zn_4$ (**I**) (*P4/mbm*, a = 7.986(1) Å, c = 7.971(1) Å) and the average structure of $Na_{0.72(4)}Au_2Zn_2$ (**II**), (*P4/mbm*, a = 7.8799(6) Å, and c = 2.7326(4) Å) have clear numeric relationships with those of the parent $K_{0.37}Cd_2$ (*I4/mcm*, a = 9.169(1) Å, c = 2.8779(5) Å);[20] namely, $a_I \approx a_{II} \approx a_{K_{0.37}Cd_2}$, $c_I \approx 3c_{II} \approx 3c_{K_{0.37}Cd_2}$. The structures of **I** and **II** can be considered as the ternary 1 × 1 × 3 superstructure and a weakly incommensurate ternary version of parent $K_{0.37}Cd_2$ cell, respectively, the last of which contains only two independent atoms, 0.37 K in Wyckoff 4*c* (0 0 0) and Cd in 8*h* (x, 1 − x, $^1/_2$) sites. Both structures feature staggered interbonded sheets of alternating homoatomic Au or Zn squares that are not directly bonded within the individual sheets (see Figures 2 and 3). Accordingly, these all consist of

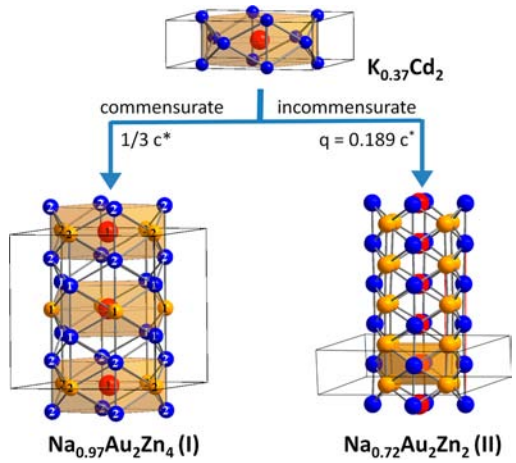

Figure 2. Structural relationships between $Na_{0.97}Au_2Zn_4$ (**I**), *P4/mbm*, and the incommensurate solution of $Na_{0.72}Au_2Zn_2$ (**II**), *P4/mbm*(00*g*)-00*ss*, compared with those of the parent $K_{0.37}Cd_2$ (*I4/mcm*). Note the incommensurate displacements within the highlighted Au and Zn chains along the channel direction in **II** (guided by red lines). For clarity, only one channel along c is shown for each structure. Red spheres represent K or simplified versions of the Na distributions (see text), and gold or blue spheres represent Au and Cd or Zn atoms. The same scheme is used for later figures.

polymer-like frameworks with 4-fold symmetry in parallel channels along c. In another viewpoint, the staggered homoatomic squares in $K_{0.37}Cd_2$ generate square antiprisms stacked in c, with every two square antiprisms (centered by K) as repeating units, as shown in the top panel in Figure 2.

The 3-fold superstructure $Na_{0.97(4)}Au_2Zn_4$, compound **I**, shown at the bottom left in Figure 2, occurs in a lower symmetry group (*P4/mbm*) with Au and Zn sheets ordered in 1: 2 proportions, the reason for the tripled c axis compared with that of the parent $K_{0.37}Cd_2$. As shown, each unit cell of **I** contains (1 + 2/2) = 2 repeating units of Au1 and Au2, as in $K_{0.37}Cd_2$ (shaded yellow) that are alternately condensed with

Table 5. Average Bond Length Ranges and Combined Molar ICOHP Values in $Na_{0.72(4)}Au_2Zn_2$ (II) (Z = 2)

bond	length (Å)	−ICOHP(avg.) (eV/per bond)	n/cell	−ICOHP (eV/cell)	contribution (%)
Au−Zn	2.636−2.744	1.26	24	30.24	70.2
Au−Au	2.733	1.45	4	5.8	13.5
Zn−Zn	2.733−2.748	0.88	6	5.28	12.2
Na−Au	3.060−3.415	0.14	8	1.12	2.6
Na−Zn	3.152−3.886	0.11	6	0.66	1.5

dx.doi.org/10.1021/ic301196z | Inorg. Chem. 2012, 51, 9395−9402

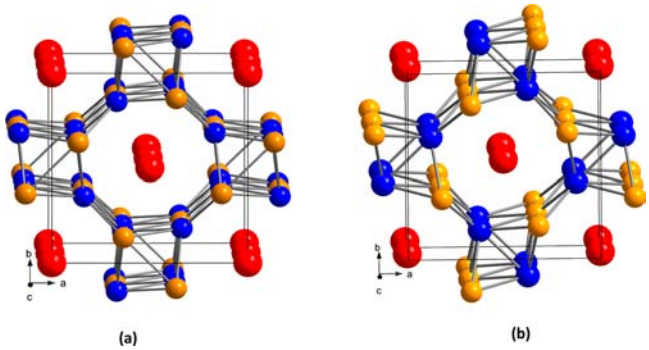

Figure 3. General ~[001] view of (a) $Na_{0.97(4)}Au_2Zn_4$ (**I**) and (b) the average $Na_{0.72(4)}Au_2Zn_2$ (**II**) with isotropic Na representations. The Zn, Au, and Na atoms are blue, orange, and red, respectively. Note that Au and Zn atoms in a 1:2 ratio are arranged in nearly linear mixed chains along *c* in panel (a) and as segregated chains in panel (b).

square antiprismatic layers of Zn, i.e., $\{(Zn2)_{4/2}(Zn1)_{4/2}\}$, which are new to the parent structure.

In comparison, the structure of $Na_{0.72(4)}Au_2Zn_2$ (II) depicted at the bottom right of Figure 2 derives directly from that of $K_{0.37}Cd_2$ on descent to *P*4 symmetry. This splits the 8*h* Cd into 4*g* and 4*h* sites of separate and equal Au and Zn square layers, each containing a mirror plane, and these are alternatively condensed in antiprismatic (staggered) sequences along *c*. Such condensation leads to direct and equal length Au−Au and Zn−Zn bonds along *b* and *c*. Although the Au−Au bonds along the tunnel direction also exist in KAu_4In_6 ($P\bar{6}m2$) and $K_{1.76}Au_6In_4$ ($I4/mcm$),[22] the latter are both 0.033 Å longer than the 2.733 Å Au−Au and Zn−Zn contacts here, presumably because of the larger K cations. This is probably the driving force for the incommensurate modulations (curvature) of the Au and Zn chains (Figure 2) that define the tunnels in **II**, in which way the short bond distances can be better optimized.

General views of the structures of **I** and **II** along the chain (*c*) axes shown on the left (Figure 3a) and right (Figure 3b) in Figure 3 give some feeling for the antiprismatic characteristics of the tunnels but without clear details of the layering. However, it must be noted that the locations and appearances of the Na distributions in both Figures 2 and 3 are only symbolic. Their larger and less regular densities are not at all well described by the results of successive classic refinements of typical ellipsoids or multiples thereof (see Tables 2 and 3), although the overall compositions so refined appear to be close to fact, according to the high synthetic yields obtained.

Cation Descriptions. *$Na_{0.97(4)}Au_2Zn_4$.* Direct measures of the electron densities (e.d.) of the less regular but still relatively localized Na distributions in both structures were obtained from observed Fourier maps. Figure 4a shows the enlarged central region about the Au2 and Au1 planes (dashed lines) in **I**. (Two e.d. sections of **I** through the diagonals of the Au1 or Au2 squat square prisms in Figure 3a are also shown in Figure S3 in the Supporting Information to aid the understanding.) Of course, the disorders seen here are the composite of a long-range static distribution averaged over many cells. The peanut shape of the densities in the Au2 layers gives a semiquantitative impression that distinctive pairs of cations sharing a mirror plane though Au are locally somewhat disordered (large) yet still moderately well-defined at each layer. In contrast, the electron densities in Au1 layers, still mostly a peanut shape, extend somewhat into the "joint" between the Zn1 and Zn2 layers. The subtle difference between Au1 and Au2 layers and

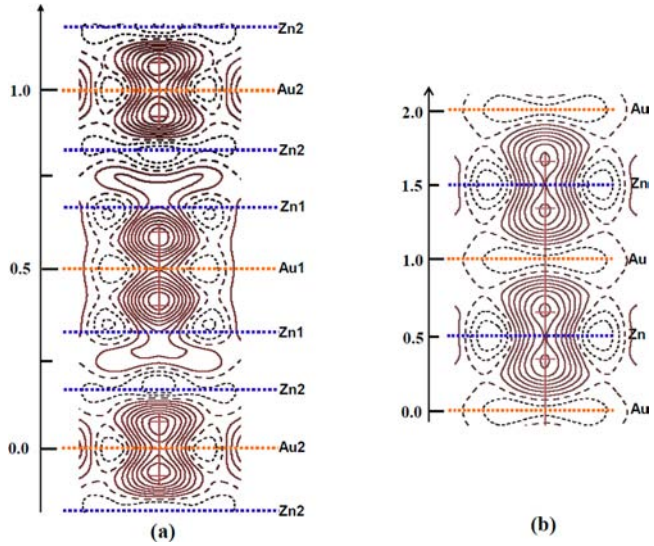

Figure 4. Observed electron density (e.d.) values along *c* in (a) $Na_{0.97(4)}Au_2Zn_4$ (**I**) and (b) $Na_{0.72(4)}Au_2Zn_2$ (**II**). Contour levels are 1.1 $e^-/Å^3$, and the length scales along *c* are the same.

their "joints" make the lattice parameter *c* triple that of $K_{0.37}Cd_2$. There are no discernible variations in the cation distributions on rotation about the 4-fold axis.

The principal reason to view these sections is to clarify the nature of the fractional Na valence electron distributions. In **I**, these all appear as two distinctly different, long-range binodal distributions along *c* of Na1 around Au2 layers and of Na2 around Au1 layers, shapes that would naturally be poorly described by the usual centric displacement ellipsoids. Obviously, the Na distributions owe their gross binodal distributions to the occurrence of both the columnar cavities (tunnels) and nearby squares of Au atoms which share the common mirror plane. More importantly, strong repulsions between the dual Na sites and a high-energy state would be expected were both valence orbitals simultaneously occupied inasmuch as these are separated by ~1.59 and ~2.39 Å at Au2 and Au1, respectively, as measured from the map (peak to peak). However, electron counting according to the (classically refined) 48.7(12)% average occupancy of all split Na sites in **I** would still allow independent full occupancy of 50% of nonadjacent pair members over the long range. In accord, there appears to be very little electron density in **I** that is not within the observed Na positions. This overall situation originates with the relatively low average electron counts (<0.5 e^- per site) around degenerate pairs of Na that are moderately well bound to heavy atoms, Au in particular, in a relatively high symmetry structure. The relatively low average valence electron count per atom, 1.57, is a parallel feature.

How well the observed e.d. distributions around each Na site follow the general dimensions of the respective heavy atom cavities in **I** also seems significant. The four types of stacked 1:2 Au:Zn squares (Figure 2a) have somewhat different edge lengths—namely, Au1, 4.21 Å; Au2, 4.40 Å; Zn1, 4.42 Å; and Zn2, 4.21 Å—meaning that the apparent columns of atoms in Figure 3a are not precisely monolithic. The average ~0.2 Å differences in edge lengths result in the Au1- and Au2-based squares that are smaller and larger in *a*, respectively, and the same relationship follows for Zn2 versus Zn1. These differences are qualitatively just as can be inferred from Figure 4a: the Na distributions between the Au1 atoms are compressed along *a*

dx.doi.org/10.1021/ic301196z | *Inorg. Chem.* 2012, 51, 9395−9402

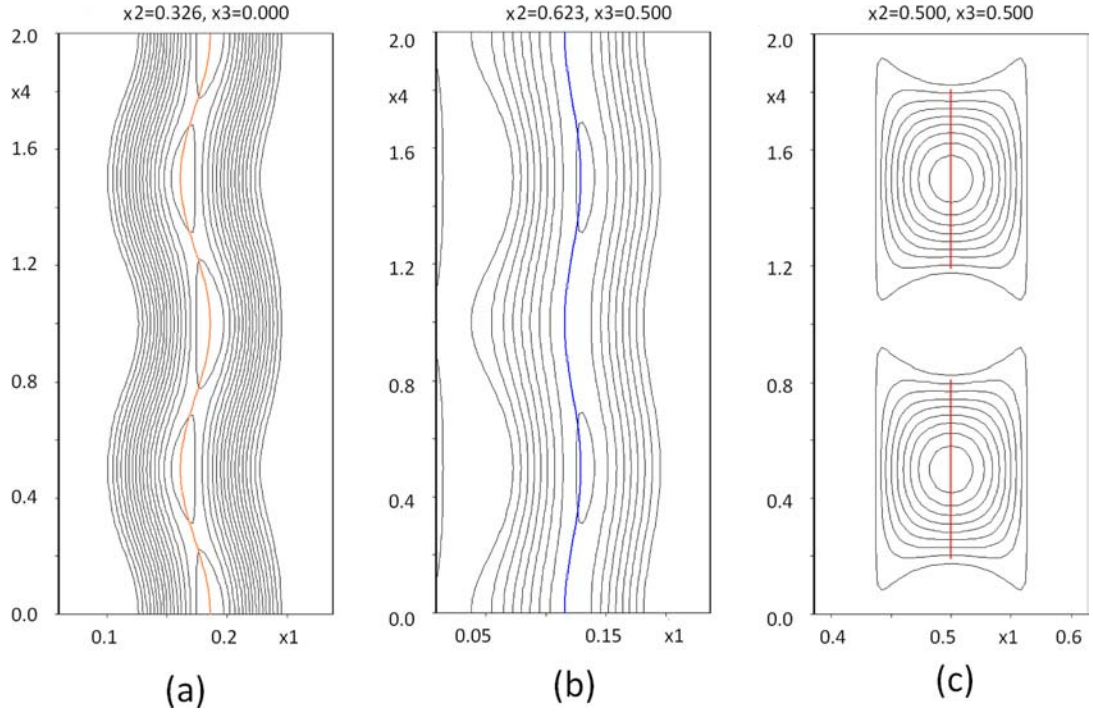

Figure 5. Observed electron densities at (a) Au, (b) Zn, and (c) Na sites in $Na_{0.72(4)}Au_2Zn_2$ (**II**) according to its refinement in superspace group *P*4/*mbm*(00*g*)00*ss*.

and expanded along *c*, and the opposite follows for the fatter distribution of Na around Au2. In other words, the somewhat soft electron distributions on the cations appear to respond fairly directly to moderate distortions in their harder network environments. It is also worth noting here that three of four independent Na−Zn distances in **I** are larger than the two different Na−Au separations (by our approximations), contrary to normal expectations for anion sizes and a forecast of what is deduced about the bonding.

$Na_{0.72(4)}Au_2Zn_2$. The simpler cell of **II** gives a different yet similar scenario. The electron densities in Figure 4b also have a peanut shape, and are also split around the mirror planes in the Zn layers when the average structure is refined. The anion lattice, a squat square prism of Au that is capped by Zn atoms (in the same sized square) on the side faces, would afford inappropriate distances for Na centered on either mirror plane. The actual distances, again measured from the peaks of the e.d. pairs, are 3.060(3) and 3.152(3) Å to Au and Zn, respectively (considering only refinement errors). Unexpectedly, these values are ∼0.05 Å *larger* than the smallest values in **I**, in which the coordination numbers are still twice as large (see Tables S5 and S6 in the Supporting Information). The random occupation of only ∼72% on average of a single site *pair* does not require as much short-range organization. With the former numbers in mind, a shrinkage or distortion of the tunnel might be required in order to shorten the homoatomic distances (Au−Au and Zn−Zn) along the tunnel direction (above), the small cation being important in this phase relative to $K_{0.37}Cd_2$.

In this case, nature selects positional modulations for Au and Zn and occupancy modulation for Na in **II**. As shown in Figure 5, the observed electron densities for Au atoms (a) and Zn atoms (b) exhibit sinuous waves along the ×4 axis, parallel to the *c*-direction, whereas the densities for Na are in isolated domains, in contrast to the peanut shapes in Figure 4b. Accordingly, Au and Zn atoms can be described by a harmonic positional modulation function, whereas Na can be described by a crenel function. The diffuse scattered reflections observed for compound **II** ($Na_{0.72(4)}Au_2Zn_2$) at ±0.189 rlu (1 rlu = 1/2.7326 $Å^{-1}$) from the Bragg planes (see Figure 1) suggest that an incommensurately modulated structure with multiplicity of 5.29 along the (001) and a complete lack of long-range order exists. As shown in Figure 2, curvatures are observed in direct space along the Au−Au and Zn−Zn bond directions, as guided by the red lines. As a consequence, Na atoms in the sinuous tunnels are better "locked in".

A common alternate explanation for such a relatively localized cation distribution in a tunnel is that these may represent tight spots in irregular tunnel walls that lead to physical trapping. This appears unlikely here for several reasons. The edges of the squares in **II** are 4.11 (Au) and 4.42 Å (Zn) (center to center), respectively, and the former, with the presumably larger van der Waals radius, might be judged the more likely barrier to physical diffusion of Na. However, the very appearance of the cation electron distributions in both e.d. maps give clear impressions that these are trapped through bonding to atoms in the anion lattice, not at particularly narrow points in the tunnel. A similar conclusion also seems apt for the $A_{0.55}Au_2Ga_2$ family, A = Na to Cs, in which disorder *increases* with cation size.[13]

Electronic Structures and Bonding. As explained in the Experimental Section, the calculations were performed on two natural models in which only one of each close Na pair evidenced in the e.d. maps was included at 100% occupancy, essentially by eliminating the central mirror planes from the model and with that, the expected large repulsion/high-energy state for the hypothetical close pairs of occupied sites. The total densities of states (DOS), and the individual atom types and orbital projections per cell in idealized (stoichiometric) $NaAu_2Zn_4$ and $Na_{0.5}Au_2Zn_2$ are shown in Figures 6a−d, columns 1 and 2, along with the subsequent COHP data for

dx.doi.org/10.1021/ic301196z | *Inorg. Chem.* 2012, 51, 9395−9402

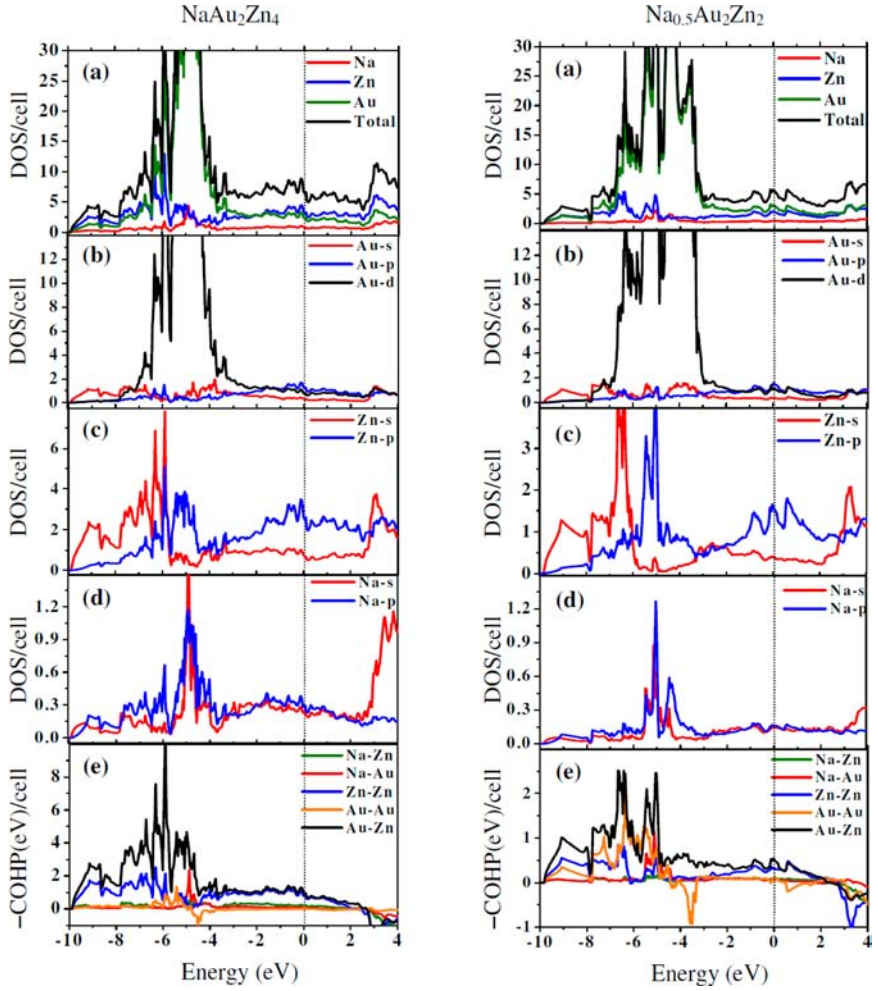

Figure 6. Results of LMTO-ASA calculations for $NaAu_2Zn_4$ (**I**) and $Na_{0.5}Au_2Zn_2$ (**II**) cells considering Zn 3d as core. (a) Density of states (DOS) for different atom types. Also shown are partial projections of orbital components (b) Au 5d,6s,6p, (c) Zn 4s,4p, and (d) Na 3s,3p. (e) OHP values (eV per cell) for Au−Zn (black), Au−Au (orange), Zn−Zn (blue), Na−Au (red), and Na−Zn (green) interactions. (The cell volumes differ by 3.0:1.)

each bond type (in Figure 6e). Significant DOS for the framework atoms at the Fermi level, for Zn especially, indicate that both compounds are metallic. The Zn 4s and 4p states fall within and below the dominant Au 5d states for both compounds. The Zn s and Zn p states are largely separated in **II**, whereas there is quite a bit of mixing between these in **I**, presumably because of the greater number of Zn interactions therein. Na 3s and 3p distributions are not differentiated in either. Major contributions at E_F come from Zn 4p and Au 6p bands in both compounds. A small valley at E_F in the DOS plot for **I** suggests that it should have full cation occupancy, essentially the refined $Na_{0.97(4)}Au_2Zn_4$, whereas the substoichiometry of **II** ($Na_{0.72}$) would back it off the peak in the DOS at E_F calculated for the stoichiometry used. According to the COHP plots, Au−Zn and Zn−Zn states remain bonding at E_F for both **I** and **II**, whereas Au−Au states are nonbonding in this region. Small but clear Na−Au bonding is seen for both whereas Na−Zn is barely visible and only in **II**, as expected.

Tables 4 and 5 summarize the respective energy-weighted averages of the Hamiltonian populations up to E_F, ICOHP, for each pairwise interaction, as well as their total bonding contributions according to the frequency of occurrence of each in the unit cells. Their analyses reveal just how dominant the numerous heteropolar Zn−Au bonds are in each phase, accounting for 63%−70% of the total per cell and averaging 1.30 and 1.26 eV/bond mol in **I** and **II**. The short Au−Au bonds in **II** and the numerous Zn−Zn contacts in **I** each make substantial contributions, 1.45 and 1.16 eV/bond mol, respectively. (The sole long Au1—Au1 bond in **I** is only incidental; see Figure 3a.) Of course, Na−Au and Na−Zn contributions are relatively small, and twice as frequent in **I**. The various bond lengths also follow the individual energy trends fairly well. Of course, it is the special relativistic effects for Au that afford additional access to the "closed" $5d^{10}$ shell in bonding and also give Au an noteworthy Mulliken electronegativity value (5.77 eV). This, in turn, can be viewed as the cause of the large bond populations for heteroatomic bonding of Au with many other metal atoms (or atoms from metals), and much new chemistry and many novel structures therefrom.[34,35]

Other Tunnel Examples. In a diffusional sense, the present rather clear results regarding cation distributions in problem 1-D tunnel structures fall near the "localized" extreme among the few other tunnel structures for which tell-tale e.d. maps are also available. The recent extremes found for $A_{0.55}Au_2Ga_2$ phases, A = Na to Cs (*I*4/*mcm*, $K_{0.5}Pt_4Si_4$-type), feature large tunnels built of planar octagonal rings of alternating Au and Ga atoms, and their e.d. maps exhibit a wide range of cation distributions

dx.doi.org/10.1021/ic301196z | *Inorg. Chem.* 2012, 51, 9395−9402

with variations of A.[12,13] The Na map shows separate but somewhat elongated density nodes (<2:1) along the tunnels with no electron density evident between them, but the e.d. maxima in the K map are separated by substantial intervening electron densities (~15%), and the distribution of Rb is substantially a continuum. (At face value, the Cs atoms show some preference for location in the heavy-atom planes.) Increases in both lattice constants and cell volumes along this $A_{0.55}$−Au_2−Ga_2 series are rather small, relative to what ion radius or volume tables usually express, leaving the clear impression that *decreases in site binding* as the cations become larger *down the group* are dominant. There are also two examples among parallel A−Au−In systems in which the implications of anisotropic ellipsoidal refinement results parallel e.d. map results;[22] the very extended ellipsoids for atoms in the tunnels parallel fairly uniform delocalization in e.d. maps for $A_{0.73}In_2In_2$ ($P4_2/nmc$), A = K, Rb, Cs, whereas extended but discrete U_{aniso} segments reflect fairly well the trimeric electron densities found by analogous mapping of $K_{1.76}Au_6In_4$($I4/mcm$).

Classical Refinement Problems with Tunnel Structures. The present e.d. maps expose some of the illusions that can arise from successive "search and refine" means for describing nonstandard atom distributions by conventional crystallography, in this case for the smaller centric Na3 and Na4 components (Table 2) that were subsequently added to the sides of the binodal Na1 and Na2 "mountains" on the mirror planes to diminish, but not to explain, leftover e.d. values. Similarly, the value of seemingly common (and easy) "solutions" of refinement problems for counterions in some tunnel structures by means of the very limited capabilities of classical anisotropic displacement ellipsoids appear to range between qualitatively consistent and undiscriminating, if not seriously misleading, depending on the finer details. For example, the relative displacement parameter ratios u_c/u_a values (the square roots of U_{33}/U_{11}) of the order of 11− 12 recently encountered with $A_{0.5}Au_2Ga_2$ tunnel structures[13] are qualitatively consistent with evidently well-delocalized cations. Otherwise, the achievement of such extreme displacement parameters for cations in tunnel structures does not ensure that these are actually well-delocalized, as in the present case.[13] A more extensive family of A−Au−In compounds exhibit parallel condensed tunnels with a wide range of cation dispositions therein.[22] Some well-localized cations owe that condition to a range of ring sizes that lead to serrated tunnel walls, whereas a range of other architectures give e.d. maps that reflect diverse degrees of cation clustering or extended delocalization. The physical meaning of extremely anisotropic parameters is difficult to understand in cases in which these extended descriptions of e.d. extend over multiple cations and approach the shapes of the tunnels.

■ ASSOCIATED CONTENT

Ⓢ Supporting Information

Table S1, Additional data regarding the incommensurate refinement; Table S2, modulation parameters for incommensurate refinement of **II**; Tables S3−S6, anisotropic thermal parameters and nearest-neighbor distances in $Na_{0.97(4)}Au_2Zn_4$ (**I**) and $Na_{0.72(4)}Au_2Zn_2$ (**II**); Figure S1, powder X-ray diffraction data for $Na_{0.97(4)}Au_2Zn_4$ (**I**) and $Na_{0.72(4)}Au_2Zn_2$ (**II**); Figure S2, positions of conventionally refined Na atoms (Table 2) on e.d. map for **I**; Figure S3, F_0 and F_c for incommensurate diffraction data; Figure S4, two longer-range electron density sections for $Na_{0.97(4)}Au_2Zn_4$ (**I**). This material is available free of charge via the Internet at http://pubs.acs.org.

■ AUTHOR INFORMATION

Corresponding Author

*E-mail: jcorbett@iastate.edu.

Notes

The authors declare no competing financial interest.

■ ACKNOWLEDGMENTS

We are grateful to G. J. Miller for guidance on calculations with paired cation distributions. This research was supported by the Office of the Basic Energy Sciences, Materials Sciences Division, U.S. Department of Energy (DOE). Ames Laboratory is operated for DOE by Iowa State University, under Contract No. DE-AC02-07CH11358.

■ REFERENCES

(1) Corbett, J. D. In *Chemistry, Structure and Bonding of Zintl Phases and Ions*; Kauzlarich, S., Ed.; VCH Publishers: New York, 1996, Chapter 3.
(2) Schafer, H.; Eisenmann, B.; Müller, W. *Angew. Chem., Int. Ed. Engl.* **1973**, *12*, 694.
(3) Corbett, J. D. *Angew. Chem., Int. Ed.* **2000**, *39*, 670.
(4) Liu, S. F.; Corbett, J. D. *Inorg. Chem.* **2004**, *43*, 2471.
(5) Liu, S. F.; Corbett, J. D. *Inorg. Chem.* **2004**, *43*, 4988.
(6) Li, B.; Corbett, J. D. *J. Am. Chem. Soc.* **2006**, *128*, 12392.
(7) Lin, Q.; Corbett, J. D. *Inorg. Chem.* **2007**, *46*, 8722.
(8) Dai, J.-C; Corbett, J. D. *Inorg. Chem.* **2007**, *46*, 4592.
(9) Zachwieja, U. *Z. Anorg. Allg. Chem.* **1995**, *621*, 1677.
(10) Zachwieja, U. *J. Alloys Compd.* **1996**, *235*, 7.
(11) Li, B.; Corbett, J. D. *Inorg. Chem.* **2005**, *44*, 6515.
(12) Smetana, V.; Corbett, J. D.; Miller, G. J. *Inorg. Chem.* **2011**, *50*, 1695.
(13) Smetana, V.; Miller, G. J.; Corbett, J. D. *Inorg. Chem.* **2012**, *51*, 7711.
(14) Samal, S. L.; Corbett, J. D. *Inorg. Chem.* **2011**, *50*, 7033.
(15) Gupta, S.; Corbett, J. D. *Inorg. Chem.* **2012**, *51*, 2247.
(16) Samal, S.; Gulo, F.; Corbett, J. D. Unpublished research.
(17) Harms, W.; Dürr, I.; Röhr, C. *Z. Naturforsch.* **2009**, *64b*, 471.
(18) Harms, W.; Dürr, I.; Daub, M.; Röhr, C. *J. Solid State Chem.* **2010**, *183*, 157.
(19) Thronberens, W.; Sinnen, H. D.; Schuster, H. U. *J. Less-Common Met.* **1980**, *76*, 99.
(20) Todorov, E.; Sevov, S. C. *Inorg. Chem.* **1998**, *37*, 6341.
(21) Lin, Q.; Lidin, S.; Corbett, J. D. *Inorg. Chem.* **2008**, *46*, 1020.
(22) Li, B.; Corbett, J. D. *Inorg. Chem.* **2007**, *46*, 6022.
(23) Byström, A.; Byström, M. *Acta Crystallogr.* **1950**, *3*, 146.
(24) Zachwieja, U. *Z. Anorg. Allg. Chem.* **1996**, *622*, 1581.
(25) *WinXPow 2.10*; Stoe & Cie GmbH: Darmstadt, Germany, 2004.
(26) *SMART*; Bruker AXS, Inc.; Madison, WI, 1996.
(27) Blessing, R. H. *Acta Crystallogr., Sect. A: Cryst. Phys. Diffr., Theor. Gen. Crystallogr.* **1995**, *A51*, 33.
(28) *SHELXTL*; Bruker AXS, Inc.: Madison, WI, 2000.
(29) Petříček, V.; Dušek, M.; Palatinus, L. *JANA2006—The Crystallographic Computing System*; Institute of Physics: Praha, Czech Republic, 2006.
(30) Palatinus, L.; Chapuis, G. *J. Appl. Crystallogr.* **2007**, *40*, 786.
(31) Krier, G.; Jepsen, O.; Burkhardt, A.; Andersen, O. K. *TB-LMTO-ASA Program*, version 4.7; Max-Planck-Institut für Festkörperforschung: Stuttgart, Germany, 1995.
(32) Jepsen, O.; Andersen, O. K. *Z. Phys. B* **1995**, *97*, 35.
(33) Dronskowski, R.; Blöchl, P. E. *J. Phys. Chem.* **1993**, *97*, 8617.
(34) Li, B.; Kim, S.-J.; Miller, G. J.; Corbett, J. D. *Inorg. Chem.* **2009**, *48*, 6573.
(35) Corbett, J. D. *Inorg. Chem.* **2010**, *49*, 13.